EurJIC European Journal of Inorganic Chemistry
ChemPubSoc Europe
FULL PAPER

DOI:10.1002/ejic.201500138

Synthesis, Structure and Redox Properties of Asymmetric (Cyclopentadienyl)(ene-1,2-dithiolate)cobalt(III) Complexes Containing Phenyl, Pyridyl and Pyrazinyl Units

CLUSTER ISSUE

James P. Dicks,[a] Muhammad Zubair,[b] E. Stephen Davies,[a] C. David Garner,*[a] Carola Schulzke,*[c] Claire Wilson,[d] and Jonathan McMaster*[a]

Keywords: Metalloenzymes / Cofactors / Redox chemistry / Cobalt / Molybdenum / Molybdopterins / Oxygen atom transfer

The compounds [(η^5-C_5H_5)Co{SC(H)CRS}] [R = phenyl (**1**), pyridin-3-yl (**2**) or pyrazin-2-yl (**3**)] have been synthesized and characterized by elemental analysis, ^{1}H NMR, mass spectrometry and X-ray crystallography. The variation in the UV/Vis and redox properties of these compounds alone and upon acidification has been investigated. In CH_2Cl_2 solution each compound undergoes a reversible one-electron reduction, and the EPR spectrum of each monoanion has been recorded. In the presence of a 5:1 excess of trifluoroacetic acid the one-electron reduction of both **2** and **3** occurs at a less negative potential. The information obtained has been interpreted with the aid of DFT calculations for [**1**]^y, [**2**]^y and [**3**]^y (y = 0 or –1) and the monoprotonated forms [**2**H]^z and [**3**H]^z (z = +1 or 0), and this has provided insight into the nature of the redox-active orbitals in these complexes. The HOMOs and LUMOs of these species are delocalized and each involves contributions from cobalt, ene-1,2-dithiolate and R orbitals. The information from the experimental and theoretical investigations is used to suggest that, for the pyran ring-opened form of the molybdenum cofactor of oxygen-atom-transfer enzymes, the pterin may participate in the redox reactions involved in the catalytic cycle.

Introduction

Molybdenum and tungsten are the only 4d and 5d transition metals with known roles in biology. With the exceptions of the nitrogenases[1] and acetylene hydratase,[2] virtually all of the Mo- and W-containing enzymes may be viewed as catalyzing a two-electron redox reaction that involves the transfer of an oxygen atom to or from a substrate X or XO, see Equation (1).

$$XO + 2H^+ + 2e^- \rightleftharpoons X + H_2O \quad (1)$$

Biochemical investigations[3] and X-ray crystallographic studies[4] have established that, in the active sites of these enzymes, the metal is coordinated by one or two molybdopterin (MPT) ligands (Scheme 1).

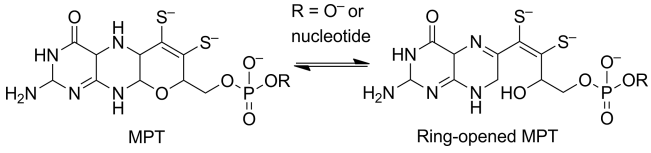

Scheme 1. Ring-closed and ring-opened forms of molybdopterin (MPT).

MPT, which is uniquely found in these enzymes, has a tricyclic structure consisting of a bicyclic pterin ring fused to a pyran ring that incorporates a $CH_2OPO_3^{2-}$ or CH_2O-$PO_2(OR)^-$ group (R = nucleotide) and an ene-1,2-dithiolate (dithiolene) unit, which coordinates the metal.[3a,5]

The Mo-containing enzymes have been classified into three families on the basis of the nature of the Mo coordination sphere at the active site in the oxidized (Mo^{VI}) form of the enzyme.[6] Members of the xanthine oxidase family each possess one MPT ligand coordinated to a *fac*-$Mo^{VI}OX(H_2O)$ (X = O or S) centre, members of the sulfite oxidase family each possess MPT coordinated to a *cis*-$Mo^{VI}O_2$ centre, which is also bound to a cysteinyl residue and H_2O, and members of the DMSO reductase family

[a] School of Chemistry, University of Nottingham, University Park, Nottingham, NG7 2RD, U.K
E-mail: dave.garner@nottingham.ac.uk
j.mcmaster@nottingham.ac.uk
http://www.nottingham.ac.uk/chemistry/people/dave.garner
http://www.nottingham.ac.uk/chemistry/people/j.mcmaster
[b] School of Chemistry, Trinity College Dublin, College Green, Dublin 2, Ireland
[c] Ernst-Moritz-Arndt-Universität, Institut für Biochemie, Arbeitskreis Bioanorganische Chemie, Felix-Hausdorff-Strasse 4, 17487 Greifswald, Germany
E-mail: schulzkec@uni-greifswald.de
http://www.mnf.uni-greifswald.de/institute/institut-fuer-biochemie/bioanorganische-chemie.html
[d] School of Chemistry, Joseph Black Building, The University of Glasgow, University Avenue, Glasgow, G12 8QQ, UK
Supporting information for this article is available on the WWW under http://dx.doi.org/10.1002/ejic.201500138.

each possess a Mo centre coordinated by two MPTs, a Mo = X (X = O or S) group plus the donor atom of an amino acid residue. Spectroscopic studies[6] have shown that the two-electron oxygen-atom-transfer (OAT) reaction [Equation (1)] catalyzed by these enzymes involves the cycling of the metal centre between the Mo^{IV} and Mo^{VI} oxidation states. In addition, the Mo^{V} state can be readily generated in many Mo-containing enzymes; studies of, for example, xanthine oxidase[7] and sulfite oxidase[8] have probed the relevance of this state in the catalytic cycles of these enzymes. The interpretation of the structural and spectroscopic studies of the catalytic centres in Mo- and W-containing enzymes has been greatly assisted by complementary investigations on a wide range of synthetic Mo and W ene-1,2-dithiolate complexes, and studies of the properties and reactions of chemical analogues of the catalytic centres of these enzymes have provided significant insights into the role of the metal centre in the catalysis of OAT by Mo- and W-containing enzymes.[9]

Although the roles of the Mo or W centres of Mo- and W-containing enzymes in the catalysis of OAT are well understood, the role of MPT remains to be defined. In the majority of the crystallographic characterizations of these enzymes, MPT exhibits extensive hydrogen bonding within the protein matrix, which might influence the geometry of the coordination sphere of the metal centre at the active site. Pterins are redox-active and may be obtained in the fully oxidized, dihydro or tetrahydro forms. The form of MPT that is found most frequently in the active sites of Mo- and W-containing enzymes characterized by X-ray crystallography involves a closed pyran ring, and the conformation resembles that of a tetrahydropterin. However, a form of MPT in which the pyran ring is open (Scheme 1) has been identified in the crystal structures of the nitrate reductase A from *Escherichia coli*[10] and ethylbenzene dehydrogenase from *Aromatoleum aromaticum*.[11] In the pyran ring-opened form of MPT the pyrazine ring of the pterin is conjugated to the ene-1,2-dithiolate unit;[12] this, together with the redox non-innocence of the ene-1,2-dithiolate group,[13] could imply that electron transfer to or from the substrate might involve the metal centre, the ene-1,2-thiolate unit *and* components of the pterin ring.[14] In support of this view, an examination of the conformations of the pyranopterin units in 102 MPT-containing X-ray crystal structures has suggested that the redox chemistry associated with this unit could support the catalytic function of the active sites of the Mo- and W-containing enzymes.[15] However, the instability of MPT outside of the protein matrix has, so far, prevented any direct study of the properties and redox chemistry of this moiety.[16] Furthermore, the synthesis of MPT represents a major chemical challenge and, although significant advances have been reported,[14e,17] further work is still required. In their synthetic studies,[17a–17f] Joule, Garner et al. used $[(\eta^5\text{-}C_5H_5)Co]^{2+}$ as the metal centre, with the organic framework being bound to this through its ene-1,2-thiolate group.[14e,17g,17h] This strategy avoided complications associated with the chemistry of $[Mo^{IV}O]^{2+}$, $[Mo^{V}O]^{3+}$ and $[Mo^{VI}O_2]^{2+}$ centres, including unwanted dimerization reactions. $[(\eta^5\text{-}C_5H_5)Co]^{2+}$ has the added advantage that it is a redox-active metal centre and undergoes a reversible one-electron reduction.[18] Thus, the properties of $[(\eta^5\text{-}C_5H_5)Co(\text{dithiolene})]$ complexes facilitate investigations of how variations in the nature of the dithiolene ligand modulate the inherent redox characteristics of the metal centre and, thereby, determine the redox properties of the complex, information of relevance to the potential role of MPT in the catalytic function of Mo- and W-containing enzymes.

In this paper we describe the synthesis, structural characterization, electrochemical and spectroscopic investigations of $[(\eta^5\text{-}C_5H_5)Co\{SC(H)CRS\}]$ [R = phenyl (**1**), pyridin-3-yl (**2**) or pyrazin-2-yl (**3**)] compounds and present DFT calculations to provide a qualitative interpretation of the information obtained. Particular attention is paid to the variation in the redox and UV/Vis and EPR spectroscopic properties of **1**, **2** and **3** in solution and of **2** and **3** in the presence of an excess of trifluoroacetic acid (TFA). The changes in the spectroscopic and redox properties of these compounds, which each possess a simplified asymmetric ene-1,2-dithiolate ligand that replicates aspects of a ring-opened MPT ene-1,2-dithiolate ligand system, are assessed as the R substituent is varied and upon acidification, with the aim of providing insights into the nature of the redox-active orbitals in these complexes.

Experimental Results

Syntheses

Each of the $[(\eta^5\text{-}C_5H_5)Co\{SC(H)CRS\}]$ compounds [R = phenyl (**1**), pyridin-3-yl (**2**) and pyrazin-2-yl (**3**)] was prepared by treating $[(\eta^5\text{-}C_5H_5)Co(CO)I_2]$ with the appropriate ene-1,2-dithiolate generated by base hydrolysis of the corresponding thione-protected 1,3-dithiolate (Scheme 2). Compound **3** was prepared from 4-pyrazin-2-yl-[1,3]dithiolene-2-one, which was itself synthesized from acetylpyrazine in three steps: (a) bromination of acetylpyrazine with 2-pyrrolidinone hydrotribromide in THF, (b) treatment of 2-pyrrolidinone hydrotribromide with potassium *O*-isopropyl carbonodithioate to yield *O*-isopropyl-*S*-[2-oxo-2-(pyrazin-2-yl)ethyl] carbonodithioate, and (c) cyclization of *O*-isopropyl-*S*-[2-oxo-2-(pyrazin-2-yl)ethyl] carbonodithioate in perchloric acid.

The structural, spectroscopic and electrochemical data for **1**, **2** and **3** reported here are consistent with the formulation of each compound as $[(\eta^5\text{-}C_5H_5)Co\{SC(H)C(R)S\}]$. In the ^1H NMR spectra the relative chemical shifts of the H^8 resonance – 9.01 ppm for **1**, 9.00 ppm for **2** and 9.55 ppm for **3** – are consistent with the nature of the ligands in respect of: (i) inductive effects, and (ii) the relative ability of the aromatic substituent to stabilize a resonance form in which a positive charge is localized at the C atom carrying the dithiolene proton. A similar order in the chemical shift of the H^8 resonances has been recognized previously for $[MO(\text{ene-1,2-dithiolate})_2]^{2-}$ (M = Mo, W) complexes.[19]

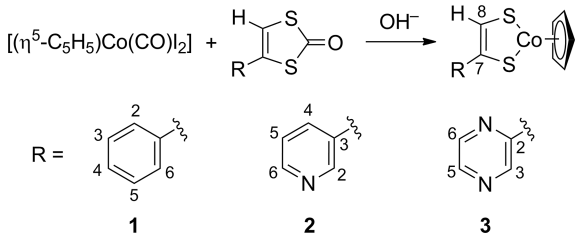

Scheme 2. Route used for the syntheses of [(η^5-C_5H_5)Co{SC(H)-CRS}] [SC(H)C(R)S, R = phenyl (**1**), pyridin-3-yl (**2**), pyrazin-2-yl (**3**)]. The numbering schemes for the various ligand substituents have been used in the assignment of the ^{1}H and ^{13}C NMR spectra of these compounds.

Structural Characterization

The structures of **1**, **2** and **3** have been determined by X-ray crystallography (see Table 1); in each case, the results obtained (Figure 1) are consistent with the corresponding molecular details shown in Scheme 2.

The {(η^5-C_5H_5)Co(SCCS)} centres of **1**, **2** and **3** are similar in nature and exhibit Co–S, C–S and dithiolene C–C interatomic distances in the ranges of 2.1025(12)–2.1224(11), 1.709(4)–1.729(4) and 1.363(3)–1.367(7) Å, respectively. Each {Co(SCCS)} unit is essentially planar, with the maximum displacement from the mean plane being ≤0.013(1) Å and the fold angle between the planes defined by Co(1)S(1)S(2) and S(1)C(1)C(2)S(2) being ≤1.79(14)° (Table 1). These metrical parameters, together with the interbond angles (Table 1), correspond to those of other compounds containing the {(η^5-C_5H_5)Co(SCCS)} unit.[18c,20] The essential equivalence in the lengths of the Co–S and C–S bonds in **1**, **2** and **3** suggests that the asymmetric nature of the ene-1,2-dithiolate ligand does not significantly affect the nature of the metal–ligand interactions. The pendant phenyl and pyridin-3-yl rings in **1** and **2** are each twisted out of the plane defined by the C(1), C(2), S(1) and S(2) atoms [ϕ = 41.3(2) and 34.00(9)° for **1** and **2**, respectively], whereas in **3** the pyrazin-2-yl ring is essentially coplanar with the SCCS unit [ϕ = 1.9(2)°].

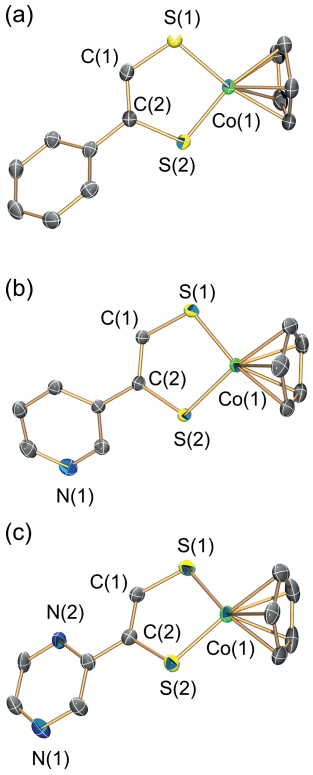

Figure 1. The molecular structures of (a) **1**, (b) **2**, and (c) **3**, with the H atoms omitted for clarity. Thermal ellipsoids are plotted at the 50% probability level.

An important aspect to the nature of a dithiolene complex is the "non-innocence" of this ligand, the two extreme forms being the ene-1,2-dithiolate ($^-$S–C=C–S$^-$) and the dithioketone (S=C–C=S).[21] Thus, the lengths of the C–C and C–S bonds can be used to comment on the nature of a dithiolene ligand in a complex. For sp^2-hybridized carbon atoms, typical bond lengths are: C–C 1.43–1.48, C=C 1.30–1.36, C–S 1.71–1.75, and C=S 1.67–1.68 Å.[22] Thus, the lengths of the C–C [1.363(3)–1.367(6) Å] and the C–S [1.705(2)–1.729(4) Å] bonds of the ligands in **1**, **2** and **3** are

Table 1. Selected bond lengths and interbond, metalladithiolene fold (θ) and ene-1,2-dithiolate/aromatic ring plane (ϕ) angles for **1**, **2** and **3**.

	1		**2**		**3**	
Bond lengths [Å]	Exp.	Calcd.	Exp.	Calcd.	Exp.	Calcd.
Co(1)–S(1)	2.1174(12)	2.129	2.1110(6)	2.131	2.1025(12)	2.132
Co(1)–S(2)	2.1224(11)	2.137	2.1195(6)	2.136	2.1092(12)	2.219
S(1)–C(1)	1.711(4)	1.715	1.705(2)	1.716	1.709(4)	1.707
S(2)–C(2)	1.729(4)	1.742	1.7280(19)	1.743	1.724(4)	1.738
C(1)–C(2)	1.367(6)	1.368	1.363(3)	1.367	1.366(6)	1.365
Bond angles [°]						
S(1)–Co(1)–S(2)	91.09(4)	91.0	91.53(2)	91.0	91.26(4)	91.1
Co(1)–S(1)–C(1)	105.16(15)	105.1	105.02(7)	105.1	105.83(14)	104.9
Co(1)–S(2)–C(2)	106.04(14)	105.9	105.30(7)	105.9	105.64(14)	105.8
S(1)–C(1)–C(2)	120.6(3)	121.1	120.47(15)	121.0	119.2(3)	121.1
S(2)–C(2)–C(1)	117.1(3)	116.9	117.68(15)	117.0	118.1(3)	117.2
θ [°]	0.82(13)	0.15	0.69(6)	0.06	1.79(14)	0.21
ϕ [°]	41.3(2)	34.95	34.00(9)	33.71	1.9(2)	4.93

consistent with the ene-1,2-dithiolate form of the dithiolene in these complexes. Therefore, to a first approximation, **1**, **2** and **3** may be formulated as [(η^5-C_5H_5)Co^{III}(ene-1,2-dithiolate)] complexes.

UV/Vis Spectroscopic Properties of 1, 2 and 3 in CH_2Cl_2 and of 2 and 3 in the Presence of an Excess of Trifluoroacetic Acid

The UV/Vis spectra of **1**, **2** and **3** in CH_2Cl_2 solution are shown in Figure 2. Each spectrum is dominated by two absorptions at ca. 17000–17100 cm^{-1} (ε = 6600–9100 $M^{-1}cm^{-1}$) and 34000–34400 cm^{-1} (ε = 23000–30000 $M^{-1}cm^{-1}$) with other absorptions between 24300 and 29400 cm^{-1} (ε = 1500–7800 $M^{-1}cm^{-1}$) appearing as shoulders on the higher-energy band.

The changes in the UV/Vis spectra of **2** and **3** in CH_2Cl_2 in the presence of a 5:1 excess of TFA are also shown in Figure 2. Upon protonation the absorptions at 17100 cm^{-1} (ε = 8800–9100 $M^{-1}cm^{-1}$) and 34000–34400 cm^{-1} (ε = 30000–26400 $M^{-1}cm^{-1}$) in both **2** and **3** show modest shifts: in **2** to 17400 (ε = 1000 $M^{-1}cm^{-1}$) and 34000 cm^{-1} (ε = 32000 $M^{-1}cm^{-1}$), and in **3** to 17400 (ε = 1000 $M^{-1}cm^{-1}$) and 34000 cm^{-1} (ε = 32000 $M^{-1}cm^{-1}$). In addition, both spectra develop a broad absorption between 26700 (ε = 7800 $M^{-1}cm^{-1}$) and 22300 cm^{-1} (ε = 7600 $M^{-1}cm^{-1}$).

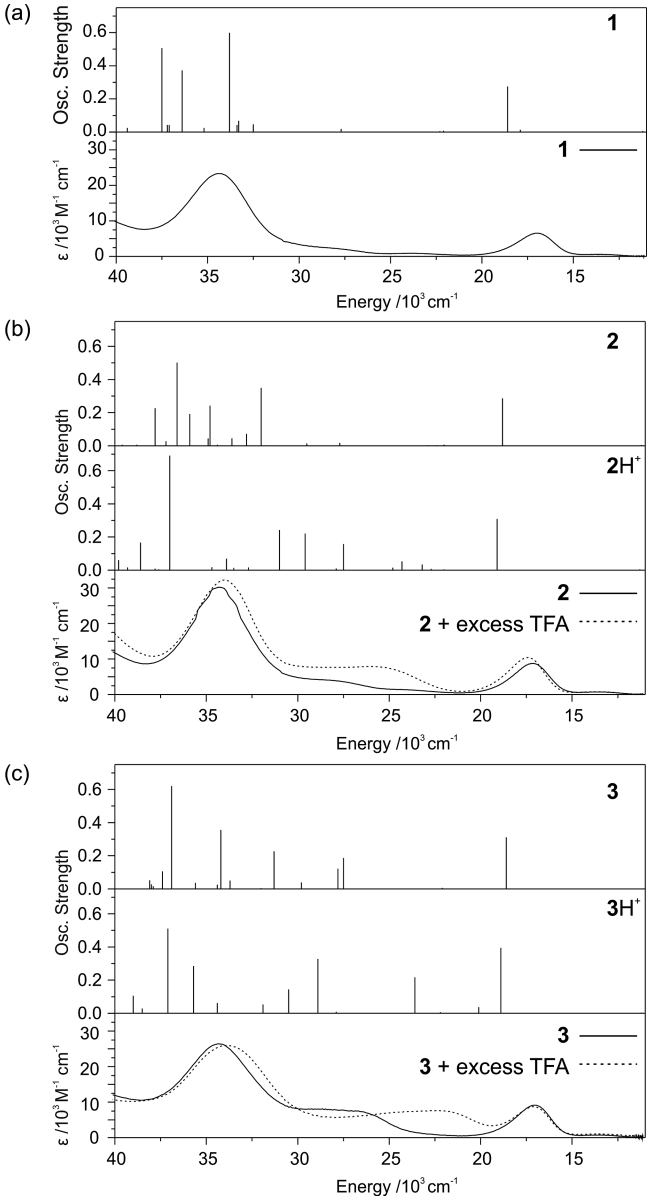

Figure 2. Observed (bottom panels) and calculated (DFT, upper panels) UV/Vis spectra of (a) **1**, (b) **2**, and (c) **3** in CH_2Cl_2, together with the corresponding information for (b) **2**, and (c) **3** in CH_2Cl_2 in the presence of a 5:1 excess of TFA. All spectra were recorded at 298 K.

Electrochemical and UV/Vis Spectroelectrochemical Properties of 1, 2 and 3 and of 2 and 3 in the Presence of an Excess of TFA

The cyclic voltammograms of **1**, **2** and **3** in CH_2Cl_2 solution containing [N*n*Bu_4][BF_4] (0.4 M) as the background electrolyte and of **2** and **3** in this medium plus a 5:1 excess of TFA were each recorded at 298 K. As in the cases of other [(η^5-C_5H_5)Co(ene-1,2-dithiolate)] complexes,[20h,23] each compound exhibited a reversible, one-electron redox couple in the range from –1.09 to –1.20 V versus Fc^+/Fc (Figure 3, Table 2).

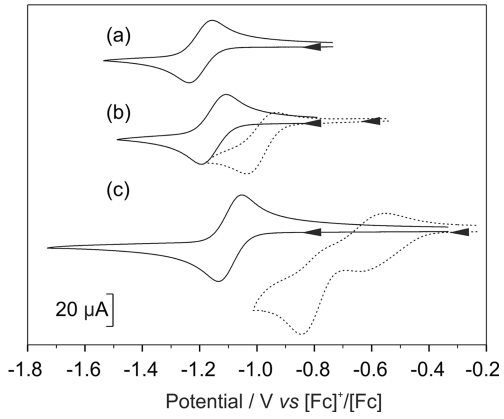

Figure 3. Cyclic voltammograms of (a) **1**, (b) **2**, and (c) **3** (1 mM, solid lines) in CH_2Cl_2 containing [N*n*Bu_4][BF_4] (0.4 M) as the background electrolyte and of (b) **2**, and (c) **3** (1 mM) in this medium with a 5:1 excess of TFA (dotted lines). The information was recorded at 298 K with use of a glassy carbon working electrode, a Pt wire secondary electrode and a saturated calomel reference electrode; potentials are expressed versus the $[Fc]^+$/[Fc] couple.

The generation of the monoanions of **1**, **2** and **3** was investigated by UV/Vis spectroelectrochemistry. In each case the one-electron reduction was accompanied by the observation of isosbestic points, consistent with reduction proceeding with no long-lived intermediates or transition states, to generate the monoanions $[\mathbf{1}]^-$, $[\mathbf{2}]^-$ and $[\mathbf{3}]^-$. At 273 K this reduction was chemically reversible (Figure 4, Table 3). The most significant spectroscopic changes involved a decrease in the intensity of the absorptions at ca.

Table 2. Potentials (vs. $[Fc]^+/[Fc]$) observed for the reduction of **1**, **2** and **3** (1 mM) in CH_2Cl_2 containing $[NnBu_4][BF_4]$ (0.4 M) as background electrolyte and of **2** and **3** (1 mM) in this medium with a 5:1 excess of trifluoroacetic acid (TFA) at room temperature.

	$E_{1/2}$ (ΔE)	E_p^c	E_p^a	ΔE (Fc^+/Fc)
1	–1.20 (0.08)			0.08
2	–1.15 (0.09)			0.09
3	–1.09 (0.08)			0.08
2 + excess TFA		–1.04	–0.94	0.09
3 + excess TFA		–0.63, –0.85	–0.56	0.08

17000–17400 and 34000–34400 cm^{-1} and an increase in the intensity of absorptions at 22900–25900 and 31100–31300 cm^{-1}.

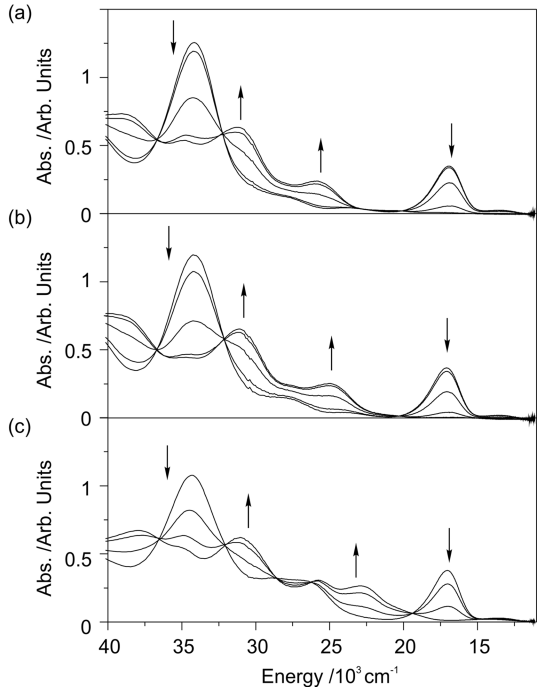

Figure 4. UV/Vis spectroscopic changes that accompany the electrochemical one-electron reduction of (a) **1**, (b) **2**, and (c) **3** in CH_2Cl_2 containing $[NnBu_4][BF_4]$ (0.4 M), recorded at an optically transparent electrode at 273 K.

The redox behaviour of **2** and **3** is significantly different in the presence of a 5:1 excess of TFA (Figure 3). Thus, the one-electron reduction of both **2** and **3** occurs at a more positive potential: **2** exhibits a reduction process at E_p^c = –1.04 V coupled to a reoxidation at E_p^a = –0.94 V (vs. Fc^+/Fc), and **3** exhibits successive reduction processes at E_p^c = –0.63 and –0.85 V vs. Fc^+/Fc coupled to a reoxidation at E_p^a = –0.56 V. Similar shifts in potentials have been observed for $[(\eta^5\text{-}C_5H_5)_2Mo\{S_2C(H)C(R)\}]$ (R = pyridin-2-yl, pyridin-3-yl or pyridin-4-yl) in the presence of HBF_4 etherate[24] and for $[(\eta^5\text{-}C_5H_5)Co\{S_2C_2H(quinoxalin\text{-}2\text{-}yl)\}]$ in the presence of TFA.[25] For the latter compound, two redox processes clearly developed, at –0.33 and –0.56 V vs. SCE, each being attributed to the one-electron redox couple of an isomer of the parent molecule formed by protonation of an N atom of the quinoxalin-2-yl ring. By analogy, the processes observed for **3** in the presence of an excess of TFA are assigned to a one-electron redox couple of one of the two isomers of $[\mathbf{3}H]^+$ that involve protonation of a pyrazin-2-yl ring N atom.

Investigations of the redox properties of **1** in the presence of an excess of TFA were not undertaken because **1** undergoes coupling reactions under acidic conditions to generate dinuclear Co-containing products.[18a]

EPR Spectroscopic Studies of the Monoanions of 1, 2 and 3

X-band EPR spectra were recorded at 77 K for electrochemically generated $[\mathbf{1}]^-$, $[\mathbf{2}]^-$ and $[\mathbf{3}]^-$ in DMF solution containing $[NnBu_4][BF_4]$ (0.2 M). The nature of the EPR spectra of these anions was essentially invariant (Figure 5) and each possesses features that are characteristic of those reported for other $[(\eta^5\text{-}C_5H_5)Co(ene\text{-}1,2\text{-}dithiolate)]^-$ species.[23a,23b,26] The EPR spectrum of $[\mathbf{1}]^-$ was simulated with rhombic spin Hamiltonian parameters (Figure 5) based on the assumptions of the unpaired electron coupling with the ^{59}Co (I = 7/2, 100%) nucleus and a coincidence of the principal *g*- and *A*-tensor axes. The latter assumption is an approximation, given the low symmetry of the Co centre, and a full interpretation of these EPR spectra, particularly the high-field features, must await single-crystal and/or multifrequency EPR experiments.[26a] Nevertheless, the interpretation of the experimentally measured spectrum requires a value for the A_{33} hyperfine coupling to the ^{59}Co nucleus that is similar to those of other $[(\eta^5\text{-}C_5H_5)Co(ene\text{-}1,2\text{-}dithiolate)]$ anions, including that derived from a dithiolene-pendant to a 18-membered S_4N_2 macrocyclic ring (g_{11} = 1.993, g_{22} = 2.043 and g_{33} = 2.246; A_{11} = 30, A_{22} = 15.5 and A_{33} = 89 G),[23b] $[Co(NO)\{S_2C_2(CN)_2\}_2]^-$ (g_{iso} = 2.063, A_{iso} = 31.9 G), $[Co(NO)\{S_2C_2(CF_3)_2\}_2]^-$ (g_{iso} = 2.059, A_{iso} = 32.9 G) and $[Co(NO)(S_2C_2Ph_2)_2]^-$ (g_{iso} = 2.050, A_{iso} = 29.4 G).[27] These values of hyperfine couplings are consistent with a SOMO that involves a relatively small contribution from Co-based orbitals (vide ultra).

Table 3. UV/Vis spectroscopic changes that accompany the electrochemical reduction of **1**, **2** and **3** in CH_2Cl_2 containing $[NnBu_4][BF_4]$ (0.4 M), recorded at an optically transparent electrode at 273 K.

	Neutral [$\times 10^3$ cm^{-1}]	Reduced [$\times 10^3$ cm^{-1}]	Isosbestic points [$\times 10^3$ cm^{-1}]
1	17.0, 29.4, 34.4	25.9, 31.3, 34.8, 39.0	32.3, 36.7
2	17.1, 24.9, 29.2, 34.4	25.1, 31.1, 34.6, 40.0	32.1, 36.7
3	17.4, 26.7, 34.0	22.9, 25.8, 31.1, 37.9	19.3, 26.3, 28.6, 32.1, 36.5

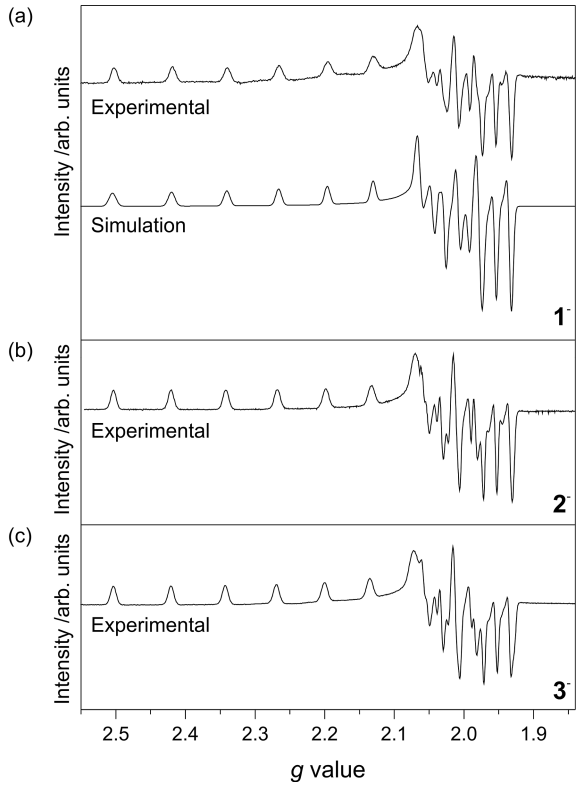

Figure 5. X-band EPR spectra of (a) [**1**]$^-$, (b) [**2**]$^-$, and (c) [**3**]$^-$ electrochemically generated from **1**, **2** and **3**, respectively, in DMF solution containing [N*n*Bu$_4$][BF$_4$] (0.2 M) at 77 K. The simulation of the EPR spectrum of [**1**]$^-$ was achieved with the spin Hamiltonian parameters g_{11} = 1993, g_{22} = 2.039 and g_{33} = 2.230, $|A_{11}|$ = 27, $|A_{22}|$ = 3 and $|A_{33}|$ = 97 × 10^{-4} cm^{-1}, with linewidths W_{11} = 39, W_{22} = 28 and W_{33} = 30 MHz. Fluid solution spectra are shown in Figure S1 in the Supporting Information and were simulated with g_{iso} = 2.092 and $|A_{iso}|$ = 37 × 10^{-4} cm^{-1}.

DFT Calculations and Discussion

We have undertaken DFT calculations for [**1**]^y, [**2**]^y and [**3**]^y (y = 0 or –1) and the monoprotonated forms [**2H**]^z and [**3H**]^z (z = +1 or 0) to provide a qualitative description of the structure and bonding within these complexes and to provide a framework for interpretation of the spectroscopic and electrochemical properties of **1**, **2** and **3** in the absence and in the presence of TFA (vide ultra). For [**3H**]^z we examined one protonated form, which involves protonation at the N(1) position (see Figure 1). Models of [**1**]^y, [**2**]^y and [**3**]^y (y = 0 or –1) and of [**2H**]^z and [**3H**]^z (z = +1 or 0) were constructed from the experimentally determined crystallographic co-ordinates for **1**, **2** and **3** before being geometry-optimized in the gas phase. Selected bond lengths and interbond angles obtained from the DFT calculations for **1**, **2** and **3** are shown in Table 1, and those for [**1**]^y, [**2**]^y and [**3**]^y (y = 0 or –1) and for [**2H**]^z and [**3H**]^z (z = +1 or 0) are listed in Table S1 in the Supporting Information.

The DFT calculations reproduce the magnitude of the crystallographically determined bond lengths, the interbond angles within the {MSCCS} metallacycle and the metalladithiolene fold angles (θ) in the structures of **1**, **2** and **3**. Thus, the CoS_2 and S_2C_2 planes are essentially coplanar both in the gas-phase theoretical and in the crystallographically determined solid-state structures. The principal difference between the calculated and the experimentally determined structures involves the dihedral angle (ϕ) between the metalladithiolene and phenyl, pyridin-3-yl or pyrazin-2-yl ring planes, the difference being ca. 6.4, 0.3 and 3.0° for **1**, **2** and **3**, respectively (Table 1).

The calculated geometrical parameters for the metalladithiolene ring for [**2H**]$^+$ and [**3H**]$^+$ (Table S1 in the Supporting Information) are similar to those of **2** and **3**, respectively (Table 1), thus suggesting that protonation does not significantly change the geometry of the metalladithiolene unit. As indicated by a comparison of the data presented in Table 1 and in Table S1 in the Supporting Information, reduction of **1**, **2** and **3** to the corresponding monoanion is accompanied by a minor lengthening of the Co–S and C–S bonds within the metalladithiolene ring, by ca. 0.05 and 0.03 Å, respectively. Also, the C–C bond increases in length by ca. 0.10 Å for the one-electron reduction of **1** and **2** but remains essentially unchanged for the reduction of **3**. Reduction of [**2H**]$^+$ to [**2H**] and of [**3H**]$^+$ to [**3H**] (Table S1 in the Supporting Information) leads to small increases in the lengths of both the Co–S and the C–S bonds.

The compositions and energies of the frontier orbitals of **1**, **2**, **3**, [**2H**]$^+$ and [**3H**]$^+$ calculated for the gas-phase geometry-optimized structures in CH_2Cl_2 solution are summarized in Table 4 and illustrated in Figure S2 in the Supporting Information. Corresponding details for the frontier orbitals of [**1**]$^-$, [**2**]$^-$, [**3**]$^-$, [**2H**] and [**3H**] are provided in Table S2 in the Supporting Information.

Each dithiolene ligand possesses four π-symmetry molecular orbitals (π_1–π_4) that resemble the butadienoid orbitals proposed for ethene-1,2-dithiolate ($S_2C_2H_2^{2-}$)[28] and filled in-plane symmetric and antisymmetric sulfur orbital combinations (σ_1 and σ_2) that may participate in σ-bonding to the metal centre.[29] The Co–dithiolene interactions within the frontier orbital manifolds of [**1**]^y, [**2**]^y and [**3**]^y (y = 0 or –1) and [**2H**]^z and [**3H**]^z (z = +1 or 0) involve principally the π_2–π_4 and σ_2 combinations (Table 4 and Table S2 in the Supporting Information, Figure S2 in the Supporting Information) and mirror those of the electronic structures calculated previously for other [(η^5-C_5H_5)Co(ene-1,2-dithiolate)] compounds.[28b,30] Thus, the HOMO in each of **1**, **2** and **3** is delocalized across the metalladithiolene unit and involves essentially Co d_{yz}, dithiolene π_3 and R group π combinations that combine in a HOMO with dithiolene (54.3–57.1%), R group (16.7–20.1%) and Co (17.4–18.0%) character. The HOMO in each of [**2H**]$^+$ and [**3H**]$^+$ has a similar composition to that of the parent compound, with dithiolene (60.9–61.5%), R group (13.4–14.8%) and Co (16.1–16.7%) character. Each of these HOMOs involves a small amount (8.2–8.6%) of Cp character. The LUMOs of **1**, **2** and **3** are essentially identical and are derived principally from Co d_{yz}, dithiolene π_3 and Cp orbital combinations. The LUMOs involve contributions from Co (44.5–45.3%) and dithiolene orbitals (27.7–29.8%), a significant contribution from Cp orbitals (23.5–23.8%) plus a minor (1.7–3.2%) contribution from the R group orbitals. The

Table 4. The nature, energy and composition of the frontier orbitals obtained from the DFT calculations for **1**, **2**, **3**, [**2**H]$^+$ and [**3**H]$^+$ in CH_2Cl_2 solution.

	Orbital designation		Nature	Energy [eV]	% Contribution Co	S_2C_2H	R	Cp
1	78a	L+3	Ph	–0.43	1.3	1.5	97.2	0.1
	77a	L+2	Ph + S_2C_2 π_4	–0.97	1.3	38.6	59.3	0.9
	76a	L+1	Co d_{xz} + S_2C_2 σ_2 + Cp	–1.73	45.9	29.0	2.3	22.8
	75a	LUMO	Co d_{yz} + S_2C_2 π_3 + Cp	–2.89	45.0	29.8	1.7	23.5
	74a	HOMO	Co d_{yz} + S_2C_2 π_3	–5.74	17.5	54.3	20.1	8.2
	73a	H-1	Co d_{xy} + S_2C_2 π_2	–6.25	45.1	49.5	2.3	3.2
2	78a	L+3	Py	–0.87	1.1	8.3	90.3	0.3
	77a	L+2	Py + S_2C_2 π_4	–1.22	2.5	28.8	67.3	1.4
	76a	L+1	Co d_{xz} + S_2C_2 σ_2 + Cp	–1.79	44.4	28.1	5.3	22.2
	75a	LUMO	Co d_{yz} + S_2C_2 π_3 + Cp	–2.93	45.3	29.1	1.8	23.8
	74a	HOMO	Co d_{yz} + S_2C_2 π_3	–5.84	18.0	57.1	16.7	8.6
	73a	H-1	Co d_{xy} + S_2C_2 π_2	–6.30	45.7	49.1	2.1	3.0
3	78a	L+3	Pz	–1.10	0.7	17.8	81.1	0.4
	77a	L+2	Co d_{xz} + S_2C_2 σ_2 + Pz	–1.82	31.8	26.7	25.6	15.8
	76a	L+1	Co d_{xz} + Pz + S_2C_2 π_4	–1.87	15.6	22.8	53.9	7.7
	75a	LUMO	Co d_{yz} + S_2C_2 π_3 + Cp	–3.01	44.5	27.7	3.2	23.7
	74a	HOMO	Co d_{yz} + S_2C_2 π_3	–5.91	17.4	56.8	17.6	8.2
	73a	H-1	Co d_{xy} + S_2C_2 π_2	–6.37	45.6	48.9	2.3	3.2
[**2**H]$^+$	78a	L+3	Py + S_2C_2 π_4	–2.00	2.1	24.2	72.6	1.1
	77a	L+2	Co d_{xz} + S_2C_2 σ_2 + Cp	–2.17	44.9	28.9	3.0	23.3
	76a	L+1	Py	–2.77	1.2	6.9	91.3	0.5
	75a	LUMO	Co d_{yz} + S_2C_2 π_3 + Cp	–3.35	45.7	24.7	4.6	24.9
	74a	HOMO	Co d_{yz} + S_2C_2 π_3	–6.33	16.7	61.5	13.4	8.4
	73a	H-1	Co d_{xy} + S_2C_2 π_2	–6.74	46.8	48.7	1.4	3.1
[**3**H]$^+$	78a	L+3	Pz + S_2C_2 π_4	–2.20	1.8	26.4	70.7	1.2
	77a	L+2	Co d_{xz} + S_2C_2 σ_2 + Cp	–2.25	46.4	28.2	0.85	24.6
	76a	L+1	Pz	–3.31	8.0	12.4	75.2	4.4
	75a	LUMO	Co d_{yz} + S_2C_2 π_3 + Cp	–3.46	38.0	18.6	22.8	20.6
	74a	HOMO	Co d_{yz} + S_2C_2 π_3	–6.41	16.1	60.9	14.8	8.2
	73a	H-1	Co d_{xy} + S_2C_2 π_2	–6.83	47.4	47.4	1.9	3.3

LUMO in [**2**H]$^+$ possesses a similar composition to that of **2** and primarily involves the Co (45.7%), dithiolene (24.7%) and Cp (24.9%) orbitals with a small (4.6%) contribution from the pyridin-3-yl orbitals. However, the LUMO in [**3**H]$^+$ possesses a greater pyrazin-2-yl character (22.8%) than that in the parent compound (17.6%), in addition to contributions from Co (38.0%), dithiolene (24.7%) and Cp (20.6%) orbitals.

The composition of the LUMO+1 orbital varies within the parent compounds. Thus, in **1** and **2** the LUMO+1 possesses Co (44.4–45.9%), dithiolene (29.0–28.1%) and Cp (22.2–22.8%) character; however, for **3** this orbital has considerable (53.9%) pyrazin-2-yl character with modest contributions from Co (15.6%), dithiolene (22.8%) and Cp (3.2%) orbitals. The LUMO+1 orbital in [**2**H]$^+$ and [**3**H]$^+$ is essentially localized on the R group and has pyridin-3-yl (91.3%) and pyrazin-2-yl (75.2%) character with only minor contributions from Co (1.2 and 8.0%, respectively) and dithiolene (6.9 and 12.4, respectively) orbitals. The LUMO+2 orbital in **1** and **2** is ligand-based with major contributions from the R group (59.3–67.3%) and the dithiolene (28.8–38.6%) orbitals. However, in **3** the LUMO+2 orbital is delocalized and involves significant contributions from the Co (31.8%) and the dithiolene (26.7%) orbitals plus contributions from orbitals on the R (25.6%) and Cp (15.8%) groups. The LUMO+2 orbital in [**2**H]$^+$ and [**3**H]$^+$ involves contributions from the Co (44.9 and 46.4%), dithiolene (28.9 and 28.2%) and Cp (23.3 and 24.6%) orbitals. The LUMO+3 in **1**, **2**, **3**, [**2**H]$^+$ and [**3**H]$^+$ possesses significant contributions from the phenyl, pyridin-3-yl or pyrazin-2-yl rings (70.7–97.2%) and also shows a similar variation in energy (ca. 1.10 eV) relative to the HOMO as observed for the energies of the LUMO+1.

The relative energies of the LUMOs of these complexes (Table 4) vary with the substituents in a manner that corresponds to the variation of the potential of the one-electron reduction (Tables 2 and 4): that is, the variation with the nature of the substituent is **1** < **2** < **3** and, also, protonation of **2** and **3** leads to an increase in the reduction potential of each compound (i.e., a shift to more positive potential).

A comparison of the experimentally measured (Figure 2) and calculated theoretical UV/Vis absorption spectra of **1**,

Table 5. Spin Hamiltonian parameters calculated by DFT for $[\mathbf{1}]^-$, $[\mathbf{2}]^-$ and $[\mathbf{3}]^-$ and those obtained by simulation of the X-band EPR spectrum of $[\mathbf{1}]^-$ recorded in DMF solution containing $[N\mathit{n}Bu_4][BF_4]$ (0.2 M) at 77 K.

Complex	g_{11}	g_{22}	g_{33}	$\lvert A_{11}\rvert$ [$\times 10^{-4}$ cm^{-1}]	$\lvert A_{22}\rvert$ [$\times 10^{-4}$ cm^{-1}]	$\lvert A_{33}\rvert$ [$\times 10^{-4}$ cm^{-1}]
$\mathbf{1}^-$ (DFT calculated)	2.004	2.026	2.137	32	15	77
$\mathbf{2}^-$ (DFT calculated)	2.005	2.025	2.137	32	15	77
$\mathbf{3}^-$ (DFT calculated)	2.007	2.027	2.138	32	15	76
$\mathbf{1}^-$ (experimental)	1.993	2.039	2.230	27	3	97

2, **3**, $[\mathbf{2H}]^+$ and $[\mathbf{3H}]^+$ in CH_2Cl_2 (Table S3 in the Supporting Information) provides support for the proposed view of the electronic structure of these complexes. The UV/Vis spectra of **1**, **2** and **3** are similar to those of other [(η^5-C_5H_5)Co(ene-1,2-dithiolate)] compounds for which the low-energy band at ca. 17000 cm^{-1} has been assigned to a HOMO to LUMO transition that involves orbitals with both ligand and metal character on the basis that the band exhibits little solvatochromism, in contrast to a transition with significant charge transfer character.[22] The LUMO – HOMO energy difference shows a relatively small variation (ca. 0.1 eV) across the series **1**, **2**, **3**, $[\mathbf{2H}]^+$ and $[\mathbf{3H}]^+$, and the low-energy band between 17000 and 17400 cm^{-1} in **1**, **2**, **3**, $[\mathbf{2H}]^+$ and $[\mathbf{3H}]^+$, which does not vary greatly in energy or intensity, is assigned to the HOMO→LUMO transition in each complex.

The calculated theoretical UV/Vis absorption spectra of **1**, **2** and **3** possess a number of transitions above ca. 27400 cm^{-1} (Figure 2 and Table S3 in the Supporting Information). Using these calculated transitions as a guide suggests that the transitions between 33900–34400 cm^{-1}, and for **1**, **2** and **3** the shoulders between 24300 to 29400 cm^{-1}, in the experimentally measured spectra (Figure 2) may be broadly assigned to intraligand charge transfer (ILCT) processes involving transitions from ene-1,2-dithiolate-based orbitals to orbitals with phenyl, pyridin-3-yl or pyrazin-2-yl π character. The absorptions around 26700 (ε = 7800 M^{-1} cm^{-1}) and 22300 cm^{-1} (ε = 7600 M^{-1} cm^{-1}) in **2** and **3**, respectively, in the presence of excess TFA are attributed to transitions between the HOMO and LUMO+1, the HOMO-1 and LUMO+1 and the HOMO and LUMO+3 of $[\mathbf{2H}]^+$ and the HOMO-1 and LUMO+1 and the HOMO and LUMO+3 of $[\mathbf{3H}]^+$. The lower energy of these transitions reflects the lower energy of the LUMO+1 and LUMO+3 orbitals when **2** and **3** are protonated.

The calculated theoretical UV/Vis absorption spectra of $[\mathbf{1}]^-$, $[\mathbf{2}]^-$ and $[\mathbf{3}]^-$ in CH_2Cl_2 solution show correspondences with the experimentally measured spectra recorded spectroelectrochemically for $[\mathbf{2H}]^+$ and $[\mathbf{3H}]^+$ in CH_2Cl_2 containing $[N\mathit{n}Bu_4][BF_4]$ (0.4 M) at 273 K, including the depletion of the relatively intense low-energy band at 17000–17100 cm^{-1} (ε = 6600–9100 M^{-1} cm^{-1}) for **1**, **2** and **3** (Figure S3 and Table S4 in the Supporting Information).

Unrestricted DFT calculations of $[\mathbf{1}]^-$, $[\mathbf{2}]^-$, $[\mathbf{3}]^-$, [**2**H] and [**3**H] indicate that the SOMOs of all these complexes are very similar and have Co d_{yz} + dithiolene π_3 + Cp character with small (6–11%) contributions from the phenyl, pyridin-3-yl or pyrazin-2-yl orbitals (Figure 6, Table S2 in the Supporting Information). The similarity in the composition of the SOMO in $[\mathbf{1}]^-$, $[\mathbf{2}]^-$ and $[\mathbf{3}]^-$ is reflected in their very similar EPR spectra (Figure 5) and the almost identical spin Hamiltonian parameters calculated for these complexes (see Table 5). The values of these parameters closely correspond to those of $[\mathbf{1}]^-$ determined by simulation of the X-band EPR spectrum of this anion recorded in DMF solution containing $[N\mathit{n}Bu_4][BF_4]$ (0.2 M) at 77 K. The small ^{59}Co (I = 7/2, 100%) hyperfine couplings reflect the relatively modest Co contribution to the SOMOs of these anions (14.5–15.7% Table S2 in the Supporting Information).

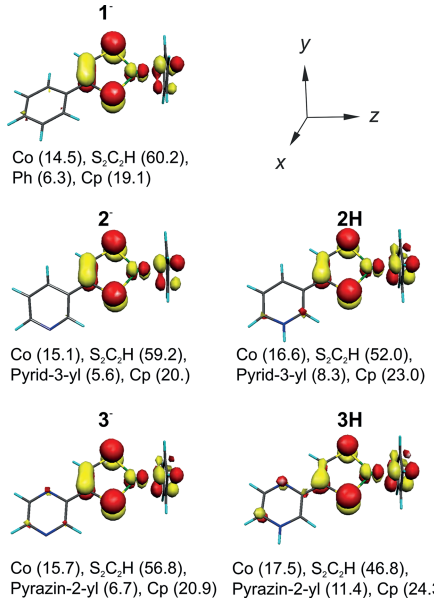

Figure 6. α-Spin Kohn–Sham frontier orbitals of $[\mathbf{1}]^-$, $[\mathbf{2}]^-$, $[\mathbf{3}]^-$, [**2**H] and [**3**H] at the 0.05 e Å^{-3} isosurface level and their percentage characters.

Conclusions

The information obtained from the structural characterization of [(η^5-C_5H_5)Co{SC(H)CRS}] [SC(H)CRS, R = phenyl (**1**), pyridin-3-yl (**2**) or pyrazin-2-yl (**3**)], their electrochemical properties alone and in the presence of a 5:1 excess of TFA, the UV/Vis spectroscopic characteristics of $[\mathbf{1}]^y$, $[\mathbf{2}]^y$ and $[\mathbf{3}]^y$ (y = 0 or –1) and of $[\mathbf{2H}]^+$ and $[\mathbf{3H}]^+$, plus the EPR spectra of $[\mathbf{1}]^-$, $[\mathbf{2}]^-$ and $[\mathbf{3}]^-$, have been successfully interpreted with the aid of information provided by DFT calculations. These calculations were concerned with the electronic structure of $[\mathbf{1}]^y$, $[\mathbf{2}]^y$ and $[\mathbf{3}]^y$ (y = 0 or –1) and of

the monoprotonated forms $[\mathbf{2H}]^z$ and $[\mathbf{3H}]^z$ (z = +1 or 0) and indicated that, in all of the species investigated, the HOMO is delocalized and involves contributions from the Co and π orbitals of the ene-1,2-dithiolate and the R substituent. The significant shift to a more positive potential for the one-electron reduction of **2** and **3** in the presence of 5 equiv. of TFA indicates that π conjugation involving an ene-1,2-thiolate unit and the R substituent (i.e., a pendant N-containing heterocyclic ring) can influence the redox properties of the metal centre without a significant change in electronic structure and bonding of the moiety.

These studies suggest that, should a form of MPT in which the pyran ring is open (Scheme 1) be integral to the catalytic cycle of the Mo- and W-enzymes, this could facilitate the participation of the pterin in the redox activity of the catalytic centres of these enzymes. In addition, given the effect of protonation on the redox behaviour of **2** and **3**, the protonation of a pyran ring-opened form of MPT could provide a mechanism for linking the proton and electron transfer that is essential for the catalytic action of the Mo- and W-oxotransferase enzymes, see Equation (1).

Experimental Section

General: All reagents were obtained from commercial sources (Aldrich Chemical Company Ltd, Lancaster Synthesis Ltd., and Fischer Scientific) and were used without further purification, unless otherwise stated. All reactions were carried out at room temperature, unless otherwise stated. All reactions that involved a metal derivative were accomplished by use of standard Schlenk line techniques under argon and with anhydrous solvents. 4-Phenyl-1,3-dithiol-2-one and 4-(pyridin-3-yl)-1,3-dithiol-2-one were prepared by literature methods.[31]

Elemental analyses were performed in the Microanalytical Laboratories of either the University of Nottingham or Ernst-Moritz-Arndt-Universität (Greifswald, Germany). IR spectra were recorded with a Nicolet Avatar 360 FTIR spectrometer. ^{1}H and ^{13}C NMR spectra were recorded with a JEOL EX270, Bruker DPX 300, Bruker DPX 400 or Bruker AV 400 spectrometer, with the chemical shifts (δ) reported in ppm. Mass spectrometry was performed with a Micromass 70E Spectrometer (EI^+). HRMS analyses were carried out with a Water-Micromass Q-ToF (quadrupole – Time of Flight) hybrid mass spectrometer equipped with an orthogonal electrospray source (z-spray) or by use of a MALDI-Q-ToF Premier system. All ToF measurements were performed at high resolution settings (5000 FWHM at mass 1500). EPR spectra were recorded with a Bruker EMX spectrometer, and spectra were simulated by use of the MATLAB toolbox EasySpin.[32]

Electrochemical measurements were performed with an Autolab PGSTAT20 potentiostat with a three-electrode configuration consisting of a saturated calomel electrode (SCE) reference electrode, a Pt wire secondary electrode and a glassy carbon working electrode. All voltammograms were recorded at ambient temperatures in CH_2Cl_2 solutions (1 mM) containing 0.4 M $[N\mathit{n}Bu_4][BF_4]$ as the supporting electrolyte and maintained under argon. All electrochemical potentials were measured relative to SCE and were corrected for liquid-junction potentials by use of the $[(\eta^5\text{-}C_5H_5)_2Fe]^+$/$[(\eta^5\text{-}C_5H_5)_2Fe]$ (Fc^+/Fc) couple as an internal redox standard. Compensation for internal resistance was not applied.

The UV/Vis spectroelectrochemical experiments were performed with an optically transparent electrochemical (OTE) cell (in a modified quartz cuvette, optical path length: 0.5 mm). A three-electrode configuration was employed; this consisted of a Pt/Rh gauze working electrode, a Pt wire secondary electrode (in a fritted PTFE sleeve), and a saturated calomel electrode (SCE) that was chemically isolated from the test solution by a bridge tube containing electrolyte solution and terminated in a porous frit. The potential at the working electrode was controlled by a Sycopel Scientific DD10M potentiostat. UV/Vis spectra were recorded on a Perkin–Elmer Lamda 16 spectrophotometer; the cavity was purged with dinitrogen, and the temperature of the sample (273 K) was controlled by flowing cooled dinitrogen across the cell surface. Sample solutions were prepared under argon by use of Schlenk line techniques; each contained $[N\mathit{n}Bu_4][BF_4]$ (0.2 M in CH_2Cl_2) as the supporting electrolyte and the compound (ca. 10^{-3} M) under investigation. The test compound was electrolysed at a constant potential, typically >100 mV more negative than E_p^c for a reduction experiment. The redox process was considered complete when consecutive spectra were identical. The chemical reversibility of the process was investigated by applying a potential at the working electrode sufficient to re-oxidize the electrogenerated product. These potentials were typically >100 mV more positive than E_p^a, to reverse a reduction process. The process was considered to be reversible if, under the conditions of the experiment, the UV/Vis profile of the starting material was reproduced at the end of the redox cycle.

Bulk electrolysis experiments, at a controlled potential, were carried out with a two-compartment cell. A Pt/Rh gauze basket working electrode was separated from a wound Pt/Rh gauze secondary electrode by a glass frit. A SCE was bridged to the test solution through a Vycor frit that was orientated at the centre of the working electrode. The working electrode compartment was fitted with a magnetic stirrer bar and the test solution was stirred rapidly during electrolysis. An ice-water bath was used to maintain a temperature of 0 °C. Each solution contained $[N\mathit{n}Bu_4][BF_4]$ (0.2 or 0.4 M) as the supporting electrolyte and the compound under investigation (10^{-3} M) and was prepared by use of Schlenk line techniques.

Details of the unit cell dimensions and of data collection and refinement for the crystal structure determinations of **1**, **2** and **3** are given in Table 6. Data for the structures of **1**, **2** and **3** were collected with a Bruker SMART APEX detector diffractometer, a Bruker SMART 1000 CCD area detector diffractometer and a Rigaku Saturn-724 diffractometer, respectively. Both Bruker systems were equipped with an Oxford Cryosystems open flow cryostat. The structures were solved by direct methods (SHELXS-97)[33] and refined against all data by full-matrix least-squares methods on F^2 (SHELXL-97).[33] All non-hydrogen atoms were refined with anisotropic displacement parameters. The hydrogen atoms were refined isotropically on calculated positions by use of a riding model with their U_{iso} values constrained to 1.2 U_{eq} of their pivotal atoms.

Restricted and unrestricted DFT calculations were performed by use of the Amsterdam Density Functional (ADF) suite version 2014.01.[34] The DFT calculations employed a Slater-type orbital (STO) all-electron triple-ζ-plus-one polarization function basis set from the ZORA/TZP database of the ADF suite for all atoms. The scalar relativistic (SR) approach was used within the ZORA Hamiltonian for the inclusion of relativistic effects, and the B3LYP hybrid functional[35] was used for the gas-phase geometry optimizations. The TDDFT calculations employed the B3LYP functional, and the conductor-like screening model (COSMO)[36] was used to estimate the effect of CH_2Cl_2 as a solvent on the electronic structure of the complexes in their gas-phase optimized geometries. Cal-

Table 6. Unit cell dimensions and data collection and refinement for the crystal structures of **1**, **2** and **3**.

	1	**2**	**3**
Empirical formula	$C_{13}H_{11}CoS_2$	$C_{12}H_{10}CoNS_2$	$C_{11}H_9CoN_2S_2$
M	290.27	291.26	292.25
Crystal system	monoclinic	monoclinic	monoclinic
Space group	$C2/c$	$P2_1/c$	$P\ 2_1/n$
a [Å]	26.372(4)	7.3456(8)	11.912(2)
b [Å]	5.7902(8)	18.783(2)	6.150(12)
c [Å]	16.324(2)	8.6882(9)	15.995(3)
α [°]	90	90	90
β [°]	107.455(2)	106.245(2)	104.84(3)
γ [°]	90	90	90
V [Å]^3	2377.9(6)	1150.9(2)	1132.8(4)
Z	8	4	4
μ [mm^{-1}]	1.760	1.820	1.852
Reflections collected	6897	2734	13030
Independent reflections	2958	2644	3382
R_{int}	0.030	0.042	0. 0364
Final R_1 [$I > 2\sigma(I)$], wR_2	0.0455, 0.1290	0.0303, 0.0726	0.0592, 0.1925

culations of the spin Hamiltonian parameters of $[\mathbf{1}]^-$, $[\mathbf{2}]^-$ and $[\mathbf{3}]^-$ used the gas-phase geometry-optimized structures and the local density approximation (LDA) with the correlation potential by Vosko et al.[37] and gradient corrections by Becke[38] and Perdew[39] (BP86). Coordinates for the initial models of $[\mathbf{1}]^y$, $[\mathbf{2}]^y$ and $[\mathbf{3}]^y$ (y = 0 or –1) and the monoprotonated forms $[\mathbf{2H}]^z$ and $[\mathbf{3H}]^z$ (z = +1 or 0) used in the gas-phase geometry optimizations were derived from the X-ray crystal structures of **1**, **2** and **3**. Within the co-ordinate frame employed in the calculations, the z-axis bisects the S–M–S angle and the x-axis lies in the CoS_2 plane. Pictorial representations of the MOs were generated with molEKEL,[40] and the orbital compositions were calculated with AOMIX.[41]

2-Bromo-1-(pyrazin-2-yl)ethanone: A solution of 2-pyrrolidinone hydrotribromide (21.8 g, 44.0 mmol) in tetrahydrofuran (80 cm^3) was added dropwise to a solution of acetylpyrazine (4.88 g, 40.0 mmol) in tetrahydrofuran (20 cm^3) over a period of 10 min. The reaction mixture was stirred for 48 h at room temperature, which resulted in a discolouration of the solution. Then the reaction mixture was cooled in an ice-bath, and cold water (30 cm^3) was added until the formed precipitates had redissolved. The aqueous layer was extracted with toluene (3 × 20 cm^3). The combined organic extracts were washed with brine (50 cm^3), dried with $MgSO_4$, filtered, and the solvents were evaporated. The obtained compound **1** was very unstable once isolated and consequently was used immediately in situ for the next step (with toluene as a solvent) without any further characterization.

***O*-Isopropyl-*S*-[2-oxo-2-(pyrazin-2-yl)ethyl] Carbonodithioate:** Potassium *O*-isopropyl carbonodithioate (7.40 g, 43.0 mmol) was added in small portions to a solution of 2-bromo-1-(pyrazin-2-yl)-ethanone (7.00 g, 35.0 mmol) in toluene (60 cm^3) over a period of 30 min. The mixture was heated under reflux for 3 h and the precipitated KBr was removed by filtration. The remaining solvent was evaporated from the reaction mixture, and then the solid residue was treated with hydrochloric acid (2.5 M, 10 cm^3) and stirred for 30 min. The aqueous layer was extracted with diethyl ether (3 × 20 cm^3). The combined organic extracts were washed with brine (50 cm^3), dried with $MgSO_4$, filtered, and the solvent was evaporated. The residue was washed with diethyl ether (2 × 10 cm^3) and dried to yield a yellowish brown solid, yield 79%, 7.10 g. Molecular formula: $C_{10}H_{12}N_2O_2S_2$ (256.34 g mol^{-1}), m.p. 98–99 °C. ^{1}H NMR ($CDCl_3$, 400 MHz, 298 K): δ_H = 8.91 (s, 1 H), 8.78 (d, J = 7.8 Hz, 1 H), 8.52 (d, J = 7.1 Hz, 1 H), 5.71 (sept, J = 6.3 Hz, 1 H), 4.79 (s, 2 H), 1.38 (d, J = 6.0 Hz, 6 H) ppm. $^{13}C\{^1H\}$ NMR ($CDCl_3$, 75 MHz, 298 K): δ_C = 215.3, 188.1, 154.8, 144.1, 143.2, 141.3, 66.3, 40.1, 23.8 ppm. IR (KBr): $\tilde{\nu}_{max}$ = 1543 (C=N), 1735 (C=O) cm^{-1}. HRMS (EI): calcd. for $C_{10}H_{12}N_2O_2S_2$ $[M + H]^+$ 257.0418; found 257.0335.

4-Pyrazin-2-yl-[1,3]dithiolene-2-one (pzdt): A solution of *O*-isopropyl-*S*-[2-oxo-2-(pyrazin-2-yl)ethyl] carbonodithioate (6.98 g, 27.3 mmol) in a mixture of diethyl ether and dichloromethane (1:1, *v*/*v*, 30 cm^3) was added slowly to a perchloric acid (70 cm^3) solution in an ice bath. The solution turned black and was allowed to warm to room temperature. After 24 h stirring, the product was precipitated by pouring into ice-cold water. The brown solid was collected by filtration and washed with distilled water (3 × 20 cm^3). The obtained brown solid was recrystallized from chloroform and dried in air for 2 h and then in an oven at 70 °C overnight, yield 47%, 2.53 g. Molecular formula: $C_7H_4N_2OS_2$ (196.24 g mol^{-1}), m.p. 140–141 °C. ^{1}H NMR ($CDCl_3$, 400 MHz, 298 K): δ_H = 8.85 (s, 1 H), 8.57 (d, J = 7.3 Hz, 1 H), 8.54 (d, J = 7.0 Hz, 1 H), 7.54 (s, 1 H) ppm. $^{13}C\{^1H\}$ NMR ($CDCl_3$, 75 MHz, 298 K): δ_C = 191.1, 145.9, 143.6, 143.2, 140.1, 132.4, 117.2 ppm. IR (KBr): $\tilde{\nu}_{max}$ = 1759 (C=O), 1544 (C=N) cm^{-1}. HRMS (ESI): calcd. for $C_7H_4N_2OS_2$ $[M + H]^+$ 196.9843; found 196.9860.

η^5-Cyclopentadienyl(1-phenyl-l,2-dithiolato)cobalt(III) (1): Compound **1** was synthesized by a modification of the procedure described by Bradshaw et al.[17e] CsOH·H_2O (0.40 g, 2.4 mmol) was dissolved in MeOH (25 cm^3), and 4-phenyl-1,3-dithiol-2-one (0.21 g, 1.1 mmol) was added. $[(\eta^5\text{-}C_5H_5)Co(CO)I_2]$ (0.44 g, 1.1 mmol) was added to the solution and a deep blue-coloured solution was obtained and was stirred for 2 h at room temperature. The solvent was then removed under vacuum, giving a black solid. This solid was extracted into ethyl acetate (4 × 50 cm^3) and the fractions were combined, after which the blue solution was filtered. The solvent was then removed from the filtrate under vacuum. The resultant black solid was dissolved in CH_2Cl_2 (30 cm^3), and *n*-hexane (20 cm^3) was added. The solution was concentrated to ca. 2 cm^3 under vacuum, resulting in the precipitation of a dark solid. The mother liquor was removed with a pipette, to leave a dark-coloured solid that was dried under vacuum, yield 109 mg, (34%). ^{1}H NMR ($CDCl_3$, 300 MHz, 298 K): δ = 9.01 (s, 1 H, 8-H), 7.78 (d, J = 7.7 Hz, 2 H, 2-H, 6-H), 7.35 (m, 3 H, 3-H, 4-H, 5-H), 5.39 ppm (s, 5 H, H^{Cp}). ^{13}C NMR ($CDCl_3$, 75 MHz, 298 K): δ = 172.4 (C-7), 155.2 (C-8), 140.1 (C-1), 128.6 (C-3, C-5), 127.5 (C-4), 126.5 (C-2, C-6), 79.3 (C^{Cp}) ppm. MS (EI): m/z = 290 [M], 188 [$C_5H_5S_2Co$], 124 [C_5H_5Co]. $C_{13}H_{10}S_2Co$ (289.28): calcd. C 53.8, H 3.8; found C 53.3, H 3.7.

η^5-Cyclopentadienyl(1-pyridin-3-yl-1,2-dithiolato)cobalt(III) (2): This compound was synthesized by a modification of procedure described by Bradshaw et al.[17e] CsOH·H_2O (0.82 g, 4.9 mmol) was dissolved in dry MeOH (20 cm^3), 4-(pyridin-3-yl)-1,3-dithiol-2-one (0.29 g, 1.5 mmol) was added, and the mixture was stirred for 5 min. $[(\eta^5\text{-}C_5H_5)Co(CO)I_2]$ (0.60 g, 1.5 mmol) was added, and the deep blue coloured solution produced was stirred for 1.5 h. After this time, the solvent was removed under vacuum and the resultant black solid was subjected to flash column chromatography (silica 60, CH_2Cl_2/MeOH 95:5, *v*/*v*). A dark blue fraction was collected as a single band, and the solvent was removed from this under vacuum, to leave a black solid. This solid was dissolved in CH_2Cl_2 (50 cm^3), and *n*-pentane was (50 cm^3) added. The solution was concentrated to a volume of ca. 2 cm^3 under vacuum, resulting in the precipitation of a dark solid. The solid was separated by removing

the mother liquor with a pipette, and dried under vacuum, yield 200 mg, (45%). ^{1}H NMR ($CDCl_3$, 300 MHz, 298 K): δ = 9.13 (br. s, 1 H, 2-H), 9.00 (s, 1 H, 8-H), 8.69 (br. s, 1 H, 6-H), 8.08 (d, J = 7.9 Hz, 1 H, 4-H), 7.28 (m, 1 H, 5-H), 5.41 ppm (s, 5 H, H^{Cp}). ^{13}C NMR ($CDCl_3$, 75 MHz, 298 K): δ = 167.9 (C-7), 155.6 (C-8), 148.5 (C-6, C-3), 147.3 (C-2), 133.4 (C-4), 124.3 (C-5), 79.5 (C^{Cp}) ppm. MS (EI): m/z = 291 [M], 188 [$C_5H_5S_2Co$], 124 [C_5H_5Co]. $C_{12}H_{10}NS_2Co$ (291.28): calcd. C 49.5, H 3.4, N, 4.8; found C 49.3, H 3.7, N 4.3.

η^5-Cyclopentadienyl(1-pyrazin-2-yl-1,2-dithiolato)cobalt(III) (3): This compound was synthesized by a modification of the procedure described by Bradshaw et al.[17e] NaOH (0.21 g, 2.5 mmol) was dissolved in dry EtOH (10 cm^3), and 4-(pyrazin-2-yl)-1,3-dithiol-2-one (0.18 g, 0.90 mmol) was added. [(η^5-C_5H_5)Co(CO)I_2] (0.40 g, 1.00 mmol) in dry EtOH (5 cm^3) was added, and the deep blue coloured solution produced was stirred overnight. After this time, the solvent was removed under vacuum, and the resultant black solid was subjected to flash column chromatography (silica 60, CH_2Cl_2/MeOH 99:1, v/v). A dark blue fraction was collected as a single band, and the solvent was removed from this under vacuum, to leave a dark blue solid. The solid was washed with methanol (2 × 10 cm^3) and dried. The product was crystallized from dichloromethane/hexane (5:2) to give blue shiny crystals that were suitable for X-ray diffraction, yield 88 mg (33%). ^{1}H NMR ($CDCl_3$, 400 MHz, 298 K): δ = 9.54 (s, 1 H, 8-H), 9.34 (s, 1 H, 3-H), 8.52 (br. s, 1 H, 5-H), 8.49 (br. s, 1 H, 6-H) 5.46 (s, 5 H, Cp) ppm. ^{13}C NMR ($CDCl_3$, 75 MHz, 298 K): δ = 165.45 (C-2), 160.18 (C-8), 151.71 (C-7), 143.96 (C-3), 142.28 (C-5), 141.33 (C-6), 79.73 (C^{Cp}) ppm. HRMS (MALDI-ToF): calcd. for $C_{11}H_{10}CoN_2S_2$ [M + H]$^+$ 292.9617; found 292.9624. $C_{11}H_9N_2S_2Co$ (292.26): calcd. C 45.20, H 3.10, N, 9.58; found C 44.89, H 3.87, N 9.37.

Supporting Information (see footnote on the first page of this article): Experimentally measured and TDDFT-calculated UV/Vis absorption bands for **1**, **2**, [**2H**]$^+$, **3** and [**3H**]$^+$, geometry-optimized bond lengths, interbond, metalladithiolene fold and dithiolene – aromatic ring plane angles for [**1**]$^-$, [**2**]$^-$, [**3**]$^-$, [**2H**]^z and [**3H**]^z (z = +1, 0), fluid X-band EPR spectra of [**1**]$^-$, [**2**]$^-$ and [**3**]$^-$, energy level diagram and pictorial representations of the Kohn–Sham frontier orbitals of **1**, **2**, [**2H**]$^+$, **3** and [**3H**]$^+$, the nature, energy and composition of the α-spin frontier orbitals of [**1**]$^-$, [**2**]$^-$, [**3**]$^-$, [**2H**] and [**3H**], experimentally measured and DFT-calculated UV/Vis spectra of [**1**]^y, [**2**]^y and [**3**]^y (y = 0 or –1), experimentally measured and TDDFT-calculated UV/Vis absorption bands for [**1**]$^-$, [**2**]$^-$ and [**3**]$^-$, and gas-phase geometry-optimized coordinates for [**1**]^y, [**2**]^y and [**3**]^y (y = 0 or –1) and [**2H**]^z and [**3H**]^z (z = +1 or 0).

CCDC-1047105 (for **1**), -1047106 (for **2**) and -1047107 (for **3**) contain the supplementary crystallographic data for this paper. These data can be obtained free of charge from The Cambridge Crystallographic Data Centre via www.ccdc.cam.ac.uk/data_request/cif.

Acknowledgments

The authors thank the European Research Council (ERC) (project MocoModels), the Engineering and Physical Sciences Research Council (EPSRC), the University of Nottingham, UK, Trinity College Dublin, Ireland, Ernst-Moritz-Arndt-Universität, Greifswald, Germany and the European Union, COST Action CM1003 for generously supporting this work.

[1] a) B. M. Hoffman, D. Lukoyanov, Z.-Y. Yang, D. R. Dean, L. C. Seefeldt, *Chem. Rev.* **2014**, *114*, 4041–4062; b) M. W. Ribbe, Y. Hu, K. O. Hodgson, B. Hedman, *Chem. Rev.* **2014**, *114*, 4063–4080.
[2] G. Seiffert, G. Ullmann, A. Messerschmidt, B. Schink, P. Kroneck, O. Einsle, *Proc. Natl. Acad. Sci. USA* **2004**, *104*, 3073–3077.
[3] a) R. R. Mendel, S. Leimkuhler, *J. Biol. Inorg. Chem.* **2015**, *20*, 337–347; b) S. Leimkuhler, M. M. Wuebbens, K. V. Rajagopalan, *Coord. Chem. Rev.* **2011**, *255*, 1129–1144.
[4] a) F. Schneider, J. Lowe, R. Huber, H. Schindelin, C. Kisker, J. Knablein, *J. Mol. Biol.* **1996**, *263*, 53–69; b) C. Kisker, H. Schindelin, D. C. Rees, *Annu. Rev. Biochem.* **1997**, *66*, 233–267; c) D. C. Rees, Y. L. Hu, C. Kisker, H. Schindelin, *J. Chem. Soc., Dalton Trans.* **1997**, 3909–3914; d) C. Kisker, H. Schindelin, D. Baas, J. Retey, R. U. Meckenstock, P. M. H. Kroneck, *FEMS Microbiol. Rev.* **1998**, *22*, 503–521; e) M. J. Romao, *Dalton Trans.* **2009**, 4053–4068; f) H. Dobbek, *Coord. Chem. Rev.* **2011**, *255*, 1104–1116.
[5] R. Hille, J. Hall, P. Basu, *Chem. Rev.* **2014**, *114*, 3963–4038.
[6] R. Hille, *Chem. Rev.* **1996**, *96*, 2757–2816.
[7] G. N. George, R. C. Bray, *Biochemistry* **1988**, *27*, 3603–3609.
[8] E. L. Klein, A. A. Belaidi, A. M. Raitsimring, A. C. Davis, T. Krämer, A. V. Astashkin, G. Neese, G. Schwarz, J. H. Enemark, *Inorg. Chem.* **2014**, *53*, 961–971.
[9] a) J. McMaster, J. M. Tunney, C. D. Garner, in: *Progress in Inorganic Chemistry: Synthesis Properties, and Applications*, vol. 52 (Ed.: E. I. Stiefel), **2004**, p. 539–583; b) R. H. Holm, E. I. Solomon, A. Majumdar, A. Tenderholt, *Coord. Chem. Rev.* **2011**, *255*, 993–1015.
[10] M. G. Bertero, R. A. Rothery, M. Palak, C. Hou, D. Lim, F. Blasco, J. H. Weiner, N. C. J. Strynadka, *Nat. Struct. Biol.* **2003**, *10*, 681–687.
[11] D. P. Kloer, C. Hagel, J. Heider, G. E. Schulz, *Structure* **2006**, *14*, 1377–1388.
[12] a) J. H. Enemark, C. D. Garner, *J. Biol. Inorg. Chem.* **1997**, *2*, 817–822; b) J. P. McNamara, J. A. Joule, I. H. Hillier, C. D. Garner, *Chem. Commun.* **2005**, 177–179.
[13] R. Eisenberg, H. B. Gray, *Inorg. Chem.* **2011**, *50*, 9741–9751.
[14] a) C. Dong, J. Yang, S. Leimkühler, M. L. Kirk, *Inorg. Chem.* **2014**, *53*, 7077–7079; b) B. Stein, M. Kirk, *J. Biol. Inorg. Chem.* **2015**, *20*, 183–194; c) R. Rothery, J. Weiner, *J. Biol. Inorg. Chem.* **2015**, *20*, 349–372; d) M. Gómez, N. Neuman, S. Dalosto, P. González, J. Moura, A. Rizzi, C. Brondino, *J. Biol. Inorg. Chem.* **2015**, *20*, 233–242; e) P. Basu, S. Burgmayer, *J. Biol. Inorg. Chem.* **2015**, *20*, 373–383.
[15] R. A. Rothery, B. Stein, M. Solomonson, M. L. Kirk, J. H. Weiner, *Proc. Natl. Acad. Sci. USA* **2012**, *109*, 14773–14778.
[16] J. L. Johnson, B. E. Hainline, K. V. Rajagopalan, *J. Biol. Chem.* **1980**, *255*, 1783–1786.
[17] a) E. M. Armstrong, M. S. Austerberry, J. H. Birks, R. L. Beddoes, M. Helliwell, J. A. Joule, C. D. Garner, *Heterocycles* **1993**, *35*, 563–568; b) A. Dinsmore, J. H. Birks, C. D. Garner, J. A. Joule, *J. Chem. Soc. Perkin Trans. 1* **1997**, 801–807; c) B. Bradshaw, A. Dinsmore, C. D. Garner, J. A. Joule, *Chem. Commun.* **1998**, 417–418; d) B. Bradshaw, D. Collison, C. D. Garner, J. A. Joule, *Chem. Commun.* **2001**, 123–124; e) B. Bradshaw, A. Dinsmore, D. Collison, C. D. Garner, J. A. Joule, *J. Chem. Soc. Perkin Trans. 1* **2001**, 3232–3238; f) F.-A. Alphonse, R. Karim, C. Cano-Soumillac, M. Hebray, D. Collison, C. D. Garner, J. A. Joule, *Tetrahedron* **2005**, *61*, 11010–11019; g) B. R. Williams, Y. Fu, G. P. A. Yap, S. J. N. Burgmayer, *J. Am. Chem. Soc.* **2012**, *134*, 19584–19587; h) I. V. Primov, A. A. Peterson, D. N. Vaccarello, P. Basu, *RSC Adv.* **2014**, *4*, 19072–19076.
[18] a) A. Sugimori, T. Akiyama, M. Kajitani, T. Sugiyama, *Bull. Chem. Soc. Jpn.* **1999**, *72*, 879–908; b) K. Wang, in: *Progress in Inorganic Chemistry: Synthesis Properties, and Applications*, vol. 52 (Ed.: E. I. Stiefel), **2003**, p. 267–314; c) N. Nomura, *Dalton Trans.* **2011**, *40*, 2112–2140.
[19] a) E. S. Davies, R. L. Beddoes, D. Collison, A. Dinsmore, A. Docrat, J. A. Joule, C. R. Wilson, C. D. Garner, *J. Chem. Soc., Dalton Trans.* **1997**, 3985–3996; b) E. S. Davies, G. M. Aston,

R. L. Beddoes, D. Collison, A. Dinsmore, A. Docrat, J. A. Joule, C. R. Wilson, C. D. Garner, *J. Chem. Soc., Dalton Trans.* **1998**, 3647–3656.
[20] a) E. M. Armstrong, M. S. Austerberry, R. L. Beddoes, M. Helliwell, J. A. Joule, C. D. Garner, *Acta Crystallogr., Sect. C: Cryst. Struct. Commun.* **1993**, *49*, 1764–1766; b) H. W. Baird, B. M. White, *J. Am. Chem. Soc.* **1966**, *88*, 4744–4745; c) R. L. Beddoes, A. Dinsmore, M. Helliwell, C. D. Garner, J. A. Joule, *Acta Crystallogr., Sect. C: Cryst. Struct. Commun.* **1997**, *53*, 213–215; d) M. R. Churchill, J. P. Fennesse, *Inorg. Chem.* **1968**, *7*, 1123–1129; e) M. Fourmigue, V. Perrocheau, *Acta Crystallogr., Sect. C: Cryst. Struct. Commun.* **1997**, *53*, 1213–1215; f) E. J. Miller, T. B. Brill, A. L. Rheingold, W. C. Fultz, *J. Am. Chem. Soc.* **1983**, *105*, 7580–7584; g) C. Takayama, M. Kajitani, T. Sugiyama, A. Sugimori, *J. Organomet. Chem.* **1998**, *563*, 161–171; h) C. Takayama, E. Suzuki, M. Kajitani, T. Sugiyama, A. Sugimori, *Organometallics* **1998**, *17*, 4341–4343.
[21] J. A. McCleverty, *Prog. Inorg. Chem.* **1968**, *10*, 49–221.
[22] F. H. Allen, O. Kennard, D. G. Watson, L. Brammer, A. G. Orpen, R. Taylor, *J. Chem. Soc. Perkin Trans. 2* **1987**, S1.
[23] a) G. Goretzki, E. S. Davies, S. P. Argent, J. E. Warren, A. J. Blake, N. R. Champness, *Inorg. Chem.* **2009**, *48*, 10264–10274; b) H. J. Hartigan, G. Seeber, A. R. Mount, L. J. Yellowlees, N. Robertson, *New J. Chem.* **2004**, *28*, 98–103; c) M. Kajitani, T. Akiyama, A. Sugimori, K. Hirakata, Y. Hoshino, Y. Satsu, G. P. Sato, K. Shimizu, M. Kaise, C. Nishihara, *J. Electroanal. Chem.* **1988**, *251*, 421–428.
[24] J. K. Hsu, C. J. Bonangelino, S. P. Kaiwar, C. M. Boggs, J. C. Fettinger, R. S. Pilato, *Inorg. Chem.* **1996**, *35*, 4743–4751.
[25] C. D. Garner, E. M. Armstrong, M. J. Ashcroft, M. S. Austerberry, J. H. Birks, D. Collison, A. J. Goodwin, L. Larsen, D. J. Rowe, J. R. Russell, in: *Molybdenum Enzymes, Cofactors, and Model Systems* (Eds.: E. I. Stiefel, D. Coucouvanis, W. E. Newton), American Chemical Society, **1993**, p. 98–113.
[26] a) F. E. Mabbs, D. Collison, *Electron Paramagnetic Resonance of d Transition Metal Compounds*, Elsevier, Amsterdam, **1992**; b) C. Takayama, M. Kajitani, T. Sugiyama, T. Akiyama, K. Shimizu, A. Sugimori, *Organometallics* **1997**, *16*, 3498–3503.
[27] J. McCleverty, N. Atherton, J. Locke, E. J. Wharton, C. J. Winscom, *J. Am. Chem. Soc.* **1967**, *89*, 6082–6092.
[28] a) S. Alvarez, R. Vicente, R. Hoffmann, *J. Am. Chem. Soc.* **1985**, *107*, 6253–6277; b) G. Periyasamy, N. A. Burton, I. H. Hillier, M. A. Vincent, H. Disley, J. McMaster, C. D. Garner, *Faraday Discuss.* **2007**, *135*, 469–488.
[29] F. E. Inscore, R. McNaughton, B. L. Westcott, M. E. Helton, R. Jones, I. K. Dhawan, J. H. Enemark, M. L. Kirk, *Inorg. Chem.* **1999**, *38*, 1401; F. E. Inscore, R. McNaughton, B. L. Westcott, M. E. Helton, R. Jones, I. K. Dhawan, J. H. Enemark, M. L. Kirk, *Inorg. Chem.* **1999**, *38*, 1401–1410.
[30] Y.-H. Cui, W. Q. Tian, J.-K. Feng, Z.-Z. Liu, W.-Q. Li, *THEOCHEM J. Mol. Struct.* **2007**, *810*, 65–72.
[31] J. M. Tunney, A. J. Blake, E. S. Davies, J. McMaster, C. Wilson, J. McMaster, *Polyhedron* **2006**, *25*, 591–598.
[32] S. Stoll, A. Schweiger, *J. Magn. Reson.* **2006**, *178*, 42–55.
[33] G. M. Sheldrick, *Acta Crystallogr., Sect. A* **2008**, *64*, 112–122.
[34] a) G. te Velde, F. M. Bickelhaupt, S. J. A. van Gisbergen, C. Fonseca Guerra, E. J. Baerends, J. G. Snijders, T. Ziegler, *J. Comput. Chem.* **2001**, *22*, 931–967; b) C. Fonseca Guerra, J. G. Snijders, G. te Velde, E. J. Baerends, *Theor. Chem. Acc.* **1998**, *99*, 391–403; c) ADF2014, Theoretical Chemistry, Vrije Universiteit, Amsterdam, The Netherlands, http://www.scm.com.
[35] P. J. Stephens, F. J. Devlin, C. F. Chabalowski, M. J. Frisch, *J. Phys. Chem.* **1994**, *98*, 11623–11627.
[36] a) A. Klamt, G. Schüürmann, *J. Chem. Soc. Perkin Trans. 2* **1993**, 799–805; b) A. Klamt, *J. Phys. Chem.* **1995**, *99*, 2224–2235; c) A. Klamt, V. Jones, *J. Chem. Phys.* **1996**, *105*, 9972–9981.
[37] S. H. Vosko, L. Wilk, M. Nusair, *Can. J. Phys.* **1980**, *58*, 1200–1211.
[38] A. D. Becke, *Phys. Rev. A* **1988**, *38*, 3098–3100.
[39] J. P. Perdew, *Phys. Rev. B* **1986**, *33*, 8822–8824.
[40] S. Portmann, H. P. Lüthi, *Chimia* **2000**, *54*, 766–770.
[41] a) S. I. Gorelsky, *AOMix: Program for Molecular Orbital Analysis*, http://www.sg-chem.net/, version 6.82, **2013**; b) S. I. Gorelsky, A. B. P. Lever, *J. Organomet. Chem.* **2001**, *635*, 187–196.

Received: February 9, 2015
Published Online: April 22, 2015

